NeuroImage: Clinical 24 (2019) 101953

Contents lists available at ScienceDirect

NeuroImage: Clinical

journal homepage: www.elsevier.com/locate/ynicl

Diffusion kurtosis and quantitative susceptibility mapping MRI are sensitive to structural abnormalities in amyotrophic lateral sclerosis

Thomas Welton[a], Jerome J. Maller[a,b], R. Marc Lebel[c], Ek T. Tan[d], Dominic B. Rowe[e,f], Stuart M. Grieve[a,f,g,*]

[a] Sydney Translational Imaging Laboratory, Heart Research Institute, Charles Perkins Centre, University of Sydney, Australia
[b] GE Healthcare, Richmond, Victoria, Australia
[c] GE Healthcare, Calgary, Alberta, Canada
[d] GE Global Research, Niskayuna, NY, USA
[e] MND Research Centre, Faculty of Medicine and Health Sciences, Macquarie University, NSW, Australia
[f] Macquarie University Hospital, Macquarie, Australia
[g] Department of Radiology, Royal Prince Alfred Hospital, Sydney, Australia

ARTICLE INFO

Keywords:
Amyotrophic lateral sclerosis (178)
Magnetic resonance imaging (120)
DWI (128)
Motor cortex (311)
Diffusion kurtosis imaging (additional)

ABSTRACT

Objective: To construct a clinical diagnostic biomarker using state-of-the-art microstructural MRI in the motor cortex of people with amyotrophic lateral sclerosis (ALS).
Methods: Clinical and MRI data were obtained from 21 ALS patients (aged 54 ± 14 years, 33% female) and 63 age- and gender-matched controls (aged 48 ± 18 years, 43% female). MRI was acquired at 3T and included T1-weighted scan (for volumetrics), arterial spin labelling (for cerebral blood flow), susceptibility-weighted angiography (for iron deposition) and multiband diffusion kurtosis imaging (for tissue microstructure). Group differences in imaging measures in the motor cortex were tested by general linear model and relationships to clinical variables by linear regression.
Results: The ALS group had mild-to-moderate impairment (disease duration: 1.8 ± 0.8 years; ALS functional rating scale 40.2 ± 6.0; forced vital capacity 83% ± 22%). No age or gender differences were present between groups. We found significant group differences in diffusion kurtosis metrics (apparent, mean, radial and axial kurtosis: $p < .01$) and iron deposition in the motor cortex ($p = .03$). Within the ALS group, we found significant relationships between motor cortex volume, apparent diffusion and disease duration (adjusted $R^2 = 0.27$, $p = .011$); and between the apparent and radial kurtosis metrics and ALS functional rating scale (adjusted $R^2 = 0.25$, $p = .033$). A composite imaging biomarker comprising kurtosis and iron deposition measures yielded a maximal diagnostic accuracy of 83% (81% sensitivity, 85% specificity) and an area-under-the-curve of 0.86.
Conclusion: Diffusion kurtosis is sensitive to early changes present in the motor region in ALS. We propose a composite imaging biomarker reflecting tissue microstructural changes in early ALS that may provide clinically valuable diagnostic information.

1. Introduction

Amyotrophic lateral sclerosis (ALS) is a rapidly-progressive neurodegenerative disorder characterized by death of the upper and lower motor neurons (Kiernan et al., 2011). Most people survive for only two to four years after diagnosis; however, survival can be extended by several months with medications and optimal clinical support. Therefore, making a definite diagnosis of ALS as early as possible is of the utmost importance. Accurate early recognition of ALS and classification into disease subtypes would greatly facilitate faster triage of appropriate care, and would also enable trials of new interventions. Early diagnosis is also especially important in ALS because the early stages of the disease are when the patient has the greatest potential to benefit from treatment (Turner et al., 2009).

Current ALS diagnosis is based on a combination of neurological examination and qualitative radiological evaluation (Brooks, 1994;

* Corresponding author at: Sydney Translational Imaging Laboratory, Heart Research Institute, D17 Charles Perkins Centre and Sydney Medical School, The University of Sydney, NSW 2006, Australia.
E-mail addresses: thomas.welton@sydney.edu.au (T. Welton), jerome.maller@ge.com (J.J. Maller), marc.lebel@ge.com (R.M. Lebel), ek.tan@ge.com (E.T. Tan), stuart.grieve@sydney.edu.au (S.M. Grieve).

https://doi.org/10.1016/j.nicl.2019.101953
Received 8 January 2019; Received in revised form 24 June 2019; Accepted 19 July 2019
Available online 22 July 2019

Miller et al., 1999). However, this paradigm is fundamentally limited: ALS is primarily a neurodegenerative disorder and clinical observations represent the "downstream" changes caused by the disease rather than the disease process per se. Similarly, conventional imaging signs of ALS used in current clinical radiology (e.g. white matter hyperintensities and atrophy of the corticospinal tracts) are highly non-specific and represent late phase changes (Turner and Modo, 2010). It is therefore pertinent to investigate ways of more directly detecting the microstructural changes occurring in the early stages of ALS. If measurable, such signals may lead to an earlier and/or more definite diagnosis and may also provide more accurate and specific ways to track disease progression over time. In turn, this would enable more timely and effective institution of management strategies and earlier enrolment into clinical trials.

Currently, the main role of conventional MRI is in differentiation of ALS from mimic disorders (Vucic et al., 2014). Some consistent cohort-level findings have been made but these lack the sensitivity and specificity for meaningful clinical use. The most robust findings include focal atrophy of cortical grey matter (GM) predominantly in the motor cortex and in temporal and frontal lobes, depending on phenotype (Chang et al., 2005; Filippini et al., 2010; Grieve et al., 2015; Turner et al., 2007); hyperintensity of the corticospinal tracts on T2-weighted images (Hecht et al., 2001; Rajagopalan and Pioro, 2017) and; changes to diffusion tensor properties and directionality in the corticospinal tracts and other white matter tracts (Bartels et al., 2008; Sach et al., 2004; Sage et al., 2007).

MRI is a rapidly changing field, and some recent advanced MRI acquisition and analysis techniques are yet to be fully evaluated in ALS. Diffusion kurtosis imaging (DKI) is a new technique capable of measuring the microstructural complexity of tissue (Steven et al., 2014). DKI is thought to be primarily impacted by glial activity, including reactive astrogliosis (Zhuo et al., 2012), but is yet to be applied in ALS. In comparable studies of neurodegenerative disease (Li et al., 2018; Struyfs et al., 2015), diffusivity is generally increased, while diffusion kurtosis is decreased. Another technique, quantitative susceptibility mapping (QSM), is sensitive to changes in local susceptibility due to the presence of diamagnetic (calcium) and paramagnetic (iron) materials. Iron deposition was reported to be elevated in the motor cortex in ALS but did not correlate with disease severity (Schweitzer et al., 2015; Costagli et al., 2016). A single study has applied arterial spin labelling (ASL) to measure tissue perfusion, finding correlations with disease severity in cingulate and frontal cortices, however this study did not image the motor cortex and used very low image resolution ($9.0 \times 5.0 \times 2.5$ mm) (Rule et al., 2010). Such advanced MRI techniques could potentially generate signal relating to disease processes occurring "upstream" of more macroscopic or indirect measures like atrophy or T2 signal, and may therefore be better able to detect early disease or sub-clinical involvement of upper motor neurons in at-risk individuals (Turner and Modo, 2010). In particular, DKI may improve our ability to characterise grey matter abnormalities, which has previously been difficult because of the isotropic diffusion profile of grey matter (Zhuo et al., 2012).

The preliminary technical aim of the present study was to test whether there are abnormalities in state-of-the-art MRI measures in the motor cortex grey matter of people with ALS and whether they reflect disease severity. Our primary clinical objective was to design a translatable composite metric for diagnosis based on these findings. We hypothesised that in the motor cortex of people with ALS: (a) iron concentration would be higher, (b) blood flow would be lower and (c) kurtosis-based measures would be decreased compared to controls, while diffusion-based metrics would be increased. We proposed that these measures would be associated with disease severity and that a biomarker based on these outcomes would be sensitive to ALS diagnosis.

2. Materials and methods

2.1. Subjects

Twenty-one people with ALS and 61 matched healthy control subjects underwent MRI and neurological assessment at Macquarie Medical Imaging, Macquarie University Hospital, New South Wales, Australia. Clinically-definite diagnosis of ALS was made according to the El Escorial criteria (Brooks, 1994; de Carvalho et al., 2008). ALS subjects were recruited from the Multidisciplinary Motor Neurone Disease Clinic at Macquarie University. Participants had no history of a psychiatric or cardiac disorder and no contraindication to MRI scanning. The ALS functional rating scale revised version (ALSFRS-R) was scored by DBR during clinical review at time of MRI scanning. Disease duration beginning at the first date of definite diagnosis was recorded from medical records. Forced Vital Capacity (FVC) was obtained via spirometry testing in the standing position (EasyOne Spirometer, Medizintechnik AG, Switzerland). Three trials were performed with the best FVC result recorded.

2.2. Standard protocol approvals and patient consents

Written informed consent was obtained from all study participants and the study had institutional ethical approval.

2.3. Image acquisition

A 3 Tesla GE Discovery MR750w MRI scanner (GE Healthcare, Milwaukee, WI) with DV25.0 software and 32-channel Nova head coil (Nova Medical, Wilmington, MA) were used to acquire the following:

- Contiguous sagittal MPRAGE T1-weighted image with prospective motion correction. The parameters were as follows: TR = 8.39 ms, TE = 3.17 ms, TI = 900 ms, flip angle = 8°, matrix = 256 × 256, 198 slices, voxel dimensions = 1 mm isotropic, acquisition time: 4:32.
- Pseudo-continuous 3D enhanced arterial spin labelling (eASL). The parameters for the labelled (perfusion-weighted) image were as follows: TR = 6592 ms, TE = 12.18 ms, TI = 1000 ms, flip angle = 111°, matrix = 128 × 128, 48 slices, voxel dimensions = 1.875 × 1.875 × 3.000 mm, post-label delay = 1000 ms, label duration = 4000 ms, acquisition time: 5:42. The image volume was positioned to cover at least one slice above the most superior portion of the cortex and the labelling plane approximately 2 cm below the imaging slab. A proton density (PD) image with the same resolution and voxel dimensions was acquired for cerebral blood flow (CBF) quantification.
- 3D multi-echo gradient-echo T2* enhanced susceptibility-weighted angiography (eSWAN). The parameters were as follows: TR = 58.1 ms, TE = 12.74 ms, flip angle = 15°, matrix = 512 × 512, 50 slices, voxel dimensions = 0.47 × 0.47 × 3.00 mm, acquisition time: 3:55. Real and imaginary components for each echo were exported for post-processing.
- Diffusion data were acquired using a multi-shell multi-band pulse sequence with a phase offset applied to each multiband component. A multiband factor of three was used resulting in 66 acquired slices. A further diffusion-weighted sequence was also acquired (six directions) along with a reversed phase-encoded (blipped) non-diffusion (b = 0) volume. The protocol comprised three shells with b-values of 700, 1000, and 2800 mm/s^2, respectively and 140 unique gradient directions. Other parameters were as follows: TR = 4323 ms, TE = 91.80 ms, flip angle = 90°, matrix = 128 × 128, voxel dimensions = 2 mm isotropic, acquisition time: 11:42. This scheme was based on those proposed by Jones, Horsfield et al. (Jones et al., 1999), in which data points are evenly

distributed over a unit sphere in Q-space.

2.4. Image analysis

A transit time corrected CBF map was quantified based on the ASL data (Dai et al., 2012) and motion artefacts in the perfusion data were reduced with a preparation sequence using adiabatic pulses (Dai et al., 2012). Phase and magnitude components from each echo of the eSWAN were processed in the Morphology-Enabled Dipole Inversion (MEDI) toolbox (Liu et al., 2012) to reconstruct QSM images that may reflect iron concentration. Raw diffusion data were unaliased using an in-house MATLAB script. The first volume (b = 0) from the first blipped sequence and the reverse-blipped sequence were extracted and processed using TOPUP followed by Eddy to correct geometric distortions and subject motion (Andersson and Sotiropoulos, 2016; Andersson et al., 2003).

FreeSurfer (version 6; http://surfer.nmr.mgh.harvard.edu) was used to automatically segment the T1-weighted image into grey-matter ROIs based on gyral and sulcal landmarks. The FreeSurfer-measured motor cortex volumes were extracted from each subject's "aparc.a2009s" stats file from the Destrieaux atlas (Destrieux et al., 2010) and normalised to (divided by) the subject's total brain volume, as extracted from the "BrainSegVol" FreeSurfer routine. Within each subject, the same ROIs were used for both DKI and diffusion scalars. These ROIs were personalised (based on the FreeSurfer output) and therefore different for each subject. Brain parenchymal fraction was measured as the ratio of brain parenchymal volume to intracranial volume.

A rigid (6 degrees of freedom) transformation between the T1-weighted brain from FreeSurfer and the perfusion-weighted image was created using FSL FLIRT and applied to the motor cortex ROIs so that a low-resolution version of the mask was overlaid on the perfusion data. The transformed mask was thresholded at 0.7 to include only voxels which contained a high proportion of GM. The mean values of voxels within the masks on the CBF image were used as our estimates for motor cortex CBF. A similar process was used to estimate the susceptibility of the motor cortex from the QSM images. Relative iron concentration was inferred as the susceptibility of the motor cortex with respect to the susceptibility of a region of no involvement (as in Schweitzer et al. (2015) and Costagli et al. (2016)), for which we chose the calcarine sulcus. The calcarine sulcus was chosen because it is relatively distant from the motor cortex geographically, it is distinct functionally, and is not conventionally thought to be involved in ALS pathology.

Diffusion kurtosis scalars were calculated using the GNC pipeline (version 3.3; GE Global Research, Niskayuna, NY, USA). In short, head motion and eddy current corrections were performed by means of rigid and cubic image registration of each diffusion volume to the non-diffusion-encoded image using Elastix (Klein et al., 2010). Gradient nonlinearity correction of diffusivity (Tan et al., 2013) was performed. Then, model-based denoising (Sperl et al., 2017) was applied to effectively remove outliers in the multi-shell diffusion data and diffusivity maps, including kurtosis maps were generated (Sprenger et al., 2016). These included the following conventional diffusion scalars: fractional anisotropy of diffusion (FA), apparent diffusion coefficient (ADC), axial diffusion (AD), radial diffusion (RD), mean diffusion (MD) and; the kurtosis scalars: FA of kurtosis (FAK), apparent kurtosis coefficient (AKC), axial kurtosis (AK), radial kurtosis (RK) and mean kurtosis (MK) (Qi et al., 2009; Tuch, 2004). The software included correction for nonlinearity intrinsic to the MRI gradients (Tan et al., 2015). An exponential ADC image was registered to the FreeSurfer brain and the resulting transformation was applied to the motor cortex masks. To limit partial volume effects, we applied two thresholds: first, a threshold of 0.7 was applied to the registered mask (thus, retaining only voxels with 80% or more overlap with the original mask) and, second, we rejected voxels with an FA $\geq$ 0.2 (i.e., those containing a substantial CSF component (Shahim et al., 2017)). Finally, the mean values of the diffusion and kurtosis scalars within the thresholded cortical masks were recorded as above.

2.5. Statistics

We classified FA/FAK and ADC/AKC as "primary" diffusion/kurtosis metrics given their wide application and accessibility. We classified the mean, radial and axial diffusivity/kurtosis metrics as "secondary" metrics which are less biologically intuitive and validated but which are still of potential value to explore.

Because ALS symptoms tend to present unilaterally, we distinguished between symptomatic and non-symptomatic sides, rather than left and right (with symptoms presenting on the left side of the body corresponding to death of the right upper motor neurons and vice-versa). The laterality of initial symptom presentation, as recorded in the patients' medical documentation was used to determine this. For controls, the average of left and right hemispheres was used.

Frequency distributions for all variables were tested for normality using Shapiro-Wilk tests. Duration of disease was the only variable to deviate significantly from a normal distribution.

Comparison of imaging measures in the symptomatic and non-symptomatic hemispheres was performed by paired two-tailed *t*-test. We also compared left and right hemisphere CBF scores in controls to test for systematic left-right effects due to variation in the B1 + field to which the ASL is sensitive.

To assess differences in imaging measures between ALS and control groups while controlling for demographic variables, a multivariate general linear model was applied, with the clinical variables as the dependent variables, the imaging measures (for the symptomatic hemisphere motor cortex) as the independent variables and age and gender as covariates. For each, we calculated the required sample size for significance in a two-tailed *t*-test, assuming equally sized groups, a power of 0.9 and an alpha of 0.05.

Based on the results of the group comparison, we formed a composite variable to combine the strongest effects, an "early diagnostic predictor". We then tested the sensitivity and specificity of this variable by analysis of the receiver operating characteristic curve to assess its ability to classify individuals into patient or control groups over a range of thresholds. Over the full range of relevant thresholds, we calculated the true positive and false positive rates. The threshold with the maximal sum of these two was determined as the optimal threshold.

To test relationships among the imaging measures, we performed Pearson correlation tests for the main imaging measures in the symptomatic hemisphere of the ALS group. These were brain parenchymal fraction, volume, CBF, iron concentration, ADC, AKC, FA, FAK and the diagnostic predictor variable. Ignoring tests between variables derived from the diffusion data (which were all strongly intercorrelated), this amounted to 26 tests. We first defined "significance" against the uncorrected alpha level, 0.05, then against the Šidák-adjusted alpha level for 26 tests, 0.00197 (Sidak, 1967).

Variables were included or excluded in linear regression models based on an exploratory univariate analysis with a *p*-value threshold of 0.1. Relationships between imaging measures and clinical variables were tested, independent of age, gender and whole-brain volume, by backwards stepwise linear regression with disease duration, ALSFRS-R and predicted FVC as the dependent variables and using 0.10 and 0.15 as the inclusion and exclusion thresholds, respectively. We confirmed that the residuals were normally-distributed for each regression.

2.6. Data availability statement

Anonymised group data and analysis algorithms can be made available upon reasonable request from a qualified investigator for the purpose of replicating procedures and results.

Table 1
Demographic and clinical information for amyotrophic lateral sclerosis (ALS) and control groups.

	ALS		Control	
	N	%	N	%
Number	21	–	61	–
Number of females	7	33	28	43
Number with left-symptomatic limb[a]	7	33	–	–

	Mean	SD	Mean	SD
Age (years)	54	14	48	18
Age of symptom onset (years)	54	13	–	–
Disease duration (years)	1.8	0.8	–	–
ALSFRS-R	40.2	6.0	–	–
FVC (% of predicted)	83	22	–	–
BPF	0.725	0.029	0.738	0.031

ALS, amyotrophic lateral sclerosis; ALSFRS-R, amyotrophic lateral sclerosis functional rating scale (revised), scored from 0 (most impaired) to 48 (no impairment); FVC, forced vital capacity; SD, standard deviation; BPF, brain parenchymal fraction.

[a] One with bulbar-only symptoms and the remaining 13 with symptoms in the right limb.

3. Results

3.1. Sample characteristics

Table 1 shows the demographic and clinical information for each group. Fig. 1 shows example slices of the kurtosis and QSM data. The ALS group was predominantly male (67%), with the laterality of onset in the limbs being predominantly on the right (67%). The control group was matched for mean age (two-tailed t-test: $t = -1.60$, $p = .112$) and number of females (chi-squared test: $\chi^2 = 0.80$, $p = .371$). Most ALS subjects were imaged within 2 years of diagnosis (mean disease duration at time of imaging: 1.8 years). Average ALSFRS-R was 40.2 ± 6.0 (out of a maximum 48, with higher scores indicating less impairment). Subject brains were not atrophied in either group, with brain parenchymal fractions of 0.725 and 0.738 for the ALS and control groups, respectively (compared to a sample-size-weighted mean brain parenchymal fraction from normative data of 0.714 (Vågberg et al., 2017)). Frequency distributions were weakly right-tailed for ALSFRS-R and predicted FVC (more patients being less impaired), left-tailed for disease duration (more patients having ALS for a shorter duration) and normal for age. Duration of disease and ALSFRS-R were non-normally distributed (Shapiro-Wilk test: $W = 0.75$, $p < .001$; $W = 0.85$, $p = .016$). Our study was powered at 0.9 for large effect sizes (for a two-tailed t-test: $\eta^2 \geq 0.14$, Cohen's $d \geq 0.82$).

3.2. Symptomatic versus non-symptomatic hemisphere

Within the ALS group, paired t-tests revealed significant hemispheric differences for motor cortex volume (symptomatic mean = 5.0 mL, non-symptomatic mean = 5.5 mL, 10%, $t = -2.84$, $p = .010$) and relative iron concentration (symptomatic mean = −6.9, non-symptomatic mean = −13.8, $t = 2.70$, $p = .015$), with the symptomatic hemisphere cortex having smaller volumes and greater iron concentrations. In contrast, no significant hemispheric differences were found for perfusion, diffusion or kurtosis measures. In controls, no hemispheric differences were detected for any imaging measure except for non-significant trends toward lower ADC ($t = -2.00$, $p = .052$) and lower AD ($t = -1.98$, $p = .055$) in the left hemisphere. Comparison of the left and right hemisphere CBF values in controls revealed no significant difference (paired t-test: $t = -0.31$, $p = .761$).

3.3. Between-group differences in imaging measures

Table 2 summarises the group differences for the imaging measures. The diffusion kurtosis measures, AKC, MK, AK and RK, were all significantly lower in the ALS group, whereas the corresponding conventional diffusion measures were not significantly different. The ALS group showed greater iron concentrations in the motor cortex. No significant motor cortex perfusion differences were detected. Accordingly, the number of subjects needed to observe a significant difference in a two-tailed t-test at a power of 0.9 was substantially reduced in all kurtosis measures compared to standard diffusion tensor metrics; for example, the performance improvement from ADC to AKC as a test translates to a 79% reduction in the required sample size from 220 subjects to 46 subjects.

Based on these findings, we reasoned that ALS diagnosis would be strongly predicted by a simple translatable metric which combined multiple imaging outcomes. We therefore defined an “early diagnostic predictor” composite variable. To do this, we first decided to include only the variables that were significant in the group comparison analysis. Because the group difference for the kurtosis metrics (MK, AK, RK and AKC) was in the same direction, they were multiplied together (each one as the average of both hemispheres to minimise biological noise because we previously showed that they were symmetric). Then, the relative iron concentration was introduced as the numerator, because its relationship in the group comparison was opposite to that of

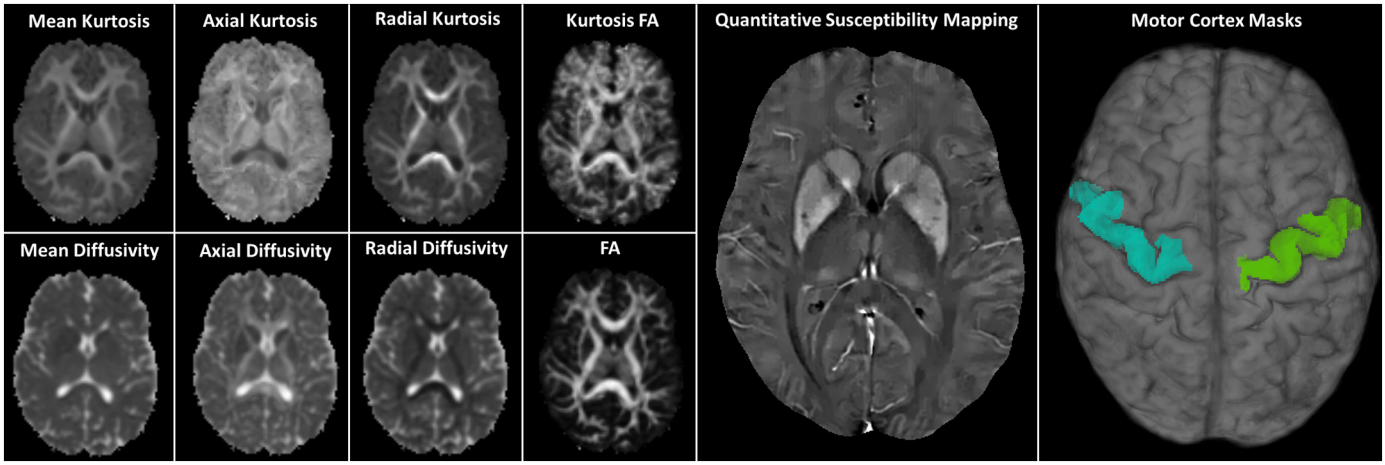

Fig. 1. Example axial slices from each of the diffusion kurtosis scalars, quantitative susceptibility mapping images and 3D motor cortex regions of interest from one control subject.

Table 2
Differences in imaging measures in the motor cortex between ALS (contralateral to the symptomatic limb) and control group (average of left and right). Results are from a multivariate GLM controlling for age and gender.

	ALS Mean (SD)	Control mean (SD)	F	p	Effect size (η2)	Required sample size for a *t*-test at 0.9 power
Non-diffusion measures						
Motor cortex volume (mm^3)	4.79×10^{-3} (3.08×10^{-4})	5.09×10^{-3} (4.72×10^{-4})	2.97	0.092	0.066	78
Blood flow (mL/100 g/min)	50.1 (9.6)	48.3 (10.2)	0.77	0.385	0.018	1276
Relative iron concentration	8.7 (7.9)	−12.5 (20.9)	5.24	0.030 *	0.168	26
Primary diffusion/Kurtosis measures						
Apparent diffusion/Kurtosis coefficient						
ADC	8.44×10^{-4} (3.17×10^{-5})	8.33×10^{-4} (1.58×10^{-5})	3.89	0.055	0.085	220
AKC	0.953 (0.049)	0.988 (0.053)	10.03	0.003 **	0.193	46
Fractional anisotropy of diffusion/Kurtosis						
FA	0.169 (0.010)	0.168 (0.017)	1.52	0.225	0.035	8178
FAK	0.149 (0.012)	0.140 (0.010)	3.61	0.064	0.079	66
Other diffusion/Kurtosis measures						
Mean diffusivity/Kurtosis						
MD	8.62×10^{-4} (2.06×10^{-4})	9.60×10^{-4} (2.04×10^{-4})	0.55	0.464	0.013	160
MK	0.744 (0.039)	0.775 (0.034)	12.28	0.001 **	0.226	76
Axial diffusivity/Kurtosis						
AD	9.93×10^{-4} (3.94×10^{-5})	9.78×10^{-4} (1.69×10^{-5})	2.36	0.132	0.053	216
AK	0.674 (0.041)	0.706 (0.026)	16.29	< 0.001 **	0.280	62
Radial diffusivity/Kurtosis						
RD	7.69×10^{-4} (2.93×10^{-5})	7.61×10^{-4} (2.01×10^{-5})	3.88	0.056	0.085	516
RK	0.811 (0.038)	0.841 (0.040)	11.29	0.002 **	0.212	90

ALS, amyotrophic lateral sclerosis; ADC, apparent diffusion coefficient; AKC, apparent kurtosis coefficient; FA, fractional anisotropy of diffusion; FAK, fractional anisotropy of kurtosis; MD, mean diffusivity; MK, mean kurtosis; AD, axial diffusion; AK, axial kurtosis; RD, radial diffusion; RK, radial kurtosis; SD, standard deviation.

* $p < 0.05$.

** $p < 0.01$.

the kurtosis metrics. For this reason, the early diagnostic predictor was constructed as a ratio of these variables, with a larger value consistent with a greater probability of disease. A negative value in the diagnostic predictor indicates a low value for relative iron concentration and a high value for kurtosis measures. Because the relative iron concentrations were often negative (i.e. the motor cortex had less iron than the calcarine sulcus), it is possible for the diagnostic predictor to also be negative.

$$\textit{Early Diagnostic Predictor} = \frac{\textit{Symptomatic Hemisphere Relative Iron Concentration}}{\left(\frac{\textit{Right AKC} + \textit{Left AKC}}{2}\right) \times \left(\frac{\textit{Right MK} + \textit{Left MK}}{2}\right) \times \left(\frac{\textit{Right RK} + \textit{Left RK}}{2}\right) \times \left(\frac{\textit{Right AK} + \textit{Left AK}}{2}\right)}$$

The early diagnostic predictor was strongly significantly different between ALS and control groups (two-tailed *t*-test: $t = 3.86$, $p < .001$; Mann-Whitney *U* test: $U = 196$, $p < .001$; Fig. 2). *Post-hoc* sensitivity and specificity analysis revealed a good classification performance using this measure (area-under-the-curve; AUC = 0.86). The optimal discrimination threshold (maximal sum of true positive and false negative rates) was a score of 0.013 (corresponding to a *z*-score of 0.3). This threshold conferred a classification performance of 81% sensitivity, 85% specificity and an accuracy of 83%. One hundred percent of cases with a score below −0.111 were controls, while 100% of cases with a score above 0.091 had ALS.

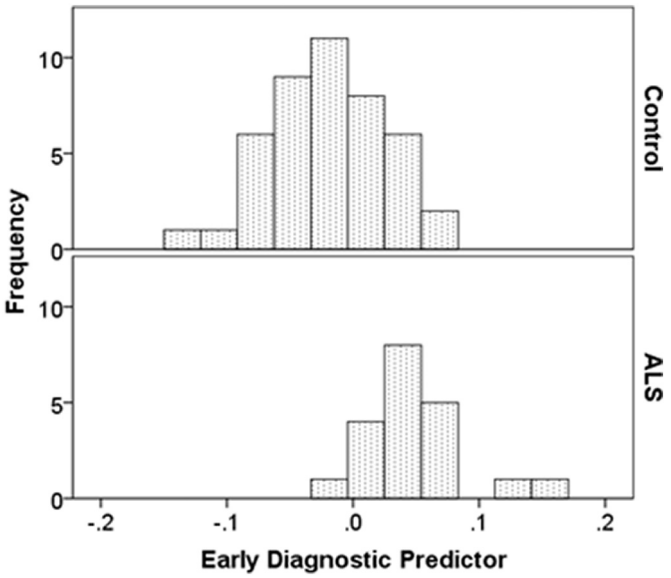

Fig. 2. Histograms comparing amyotrophic lateral sclerosis (ALS) and control groups on the early diagnostic predictor composite variable. This variable had a normal distribution for both control and ALS groups.

3.4. Relationships between imaging measures and clinical status

3.4.1. Disease duration

In the ALS group only, supra-threshold linear univariate relationships were present between disease duration and the following symptomatic hemisphere motor cortex imaging measures: volume ($r = -0.37$, $p = .095$), ADC ($r = 0.42$, $p = .065$) and FAK (-0.42, $p = .067$). No associations between relative iron concentration or perfusion and disease duration were detected. A regression model was formed to evaluate the relationship among these variables and disease duration independent of age, gender and whole-brain volume. The final model was significant and contained only motor cortex volume, FAK and ADC (adjusted $R^2 = 0.35$, $F = 4.46$, $p = .019$). The magnitude of this relationship corresponded to a 1 mL lower motor cortex volume for every year of disease duration post-diagnosis, with similarly-weighted changes in FAK and ADC (standardized coefficients: −0.35, 0.39 and −0.30, respectively).

3.4.2. Disease severity

For ALSFRS-R, the following variables had supra-threshold univariate relationships: ADC ($r = -0.38$, $p = .097$), AKC ($r = 0.42$,

$p = .068$) and RK ($r = 0.44$, $p = .050$). We confirmed that no other imaging measures were associated with disease severity by inspection of scatter plots. Backwards linear regression of ADC, AKC and RK found a good fit for a model retaining only AKC and RK (adjusted $R^2 = 0.25$, $F = 4.18$, $p = .033$), with both variables being positively related to ALSFRS-R and having similar contributions to the model (standardized coefficients: 0.37 and 0.40, respectively). The magnitude of the relationship corresponded to reductions of $Z = 0.41$ (absolute change: 0.020) in AKC and $Z = 0.42$ (absolute change: 0.022) in RK per point reduction on the ALSFRS-R.

3.4.3. FVC

For predicted FVC, there were no supra-threshold linear univariate tests. Inspection of scatter plots for non-linear trends did not identify any candidate independent variables.

3.5. Relationships among imaging measures

An exploratory analysis of relationships among the main imaging measures (ALS group symptomatic hemisphere motor cortex) revealed significant correlations between whole-brain parenchymal fraction with CBF ($r = 0.25$, $p = .039$), FA ($r = -0.25$, $p = .045$) and FAK ($r = -0.34$, $p = .006$). Volume was significantly correlated with AKC ($r = 0.29$, $p = .020$). Iron concentration was not significantly correlated with any other imaging measure. However, none of the above correlations were significant when considering multiple comparisons.

4. Discussion

Earlier and more definite diagnosis of ALS is critical for providing more effective care, subtyping and trial enrolment. MRI has the potential to provide information about the underlying microstructural changes in the brain that may precede the gross radiological signs currently used in diagnosis. We applied a cutting-edge MRI protocol in a sample of newly-diagnosed ALS patients, finding strong group-level abnormalities in multiple diffusion kurtosis-based microstructural imaging measures and relationships to disease severity. Our data informed the design of a promising composite diagnostic biomarker, which has a clinically-meaningful accuracy but which requires further validation.

The proposed early diagnostic predictor successfully distinguished ALS from control participants with a maximal accuracy of 83% and an AUC of 0.86. This compares well to a meta-analysis of imaging studies in ALS, which showed a sample size weighted mean AUC of 0.75 across 11 studies and a total of 221 patients (CI: 0.66–0.83) (Foerster et al., 2013). Our biomarker had a higher sensitivity than previous studies of 81% versus 68% (CI: 62–75%), and was comparable to the most specific test previously published by Roccatagliata, Bonzano et al. (Roccatagliata et al., 2009), who created a marker combining FA with ADC (83%, CI: 63–103%; $n = 14$). Relatively few studies have incorporated metrics derived from the motor cortex grey matter into biomarkers (Bede et al., 2017; Schuster et al., 2016). The proposed biomarker requires further investigation in larger and more clinically heterogeneous samples.

The DKI measures, AKC, MK, AK and RK (but not FAK), were abnormal in ALS, consistent with our hypothesis, and were superior to conventional tensor-based diffusion measures in differentiating ALS and control groups. The radial measures may relate to axonal diameters and the axial measures to axonal degeneration (Alexander et al., 2007), although these may be less meaningful in GM, where the axonal volume fraction is lower. That the direction and magnitude of differences varied between kurtosis and their corresponding tensor-based measures confirms that DKI provides an entirely different type of imaging metric (Steven et al., 2014). The lack of group difference in either FA or FAK suggests that the isotropic property of GM is not altered by the early effects of ALS. Kurtosis imaging allows assessment of isotropic structures (i.e., grey matter; previously a major limitation of diffusion imaging (Steven et al., 2014)), which may explain why the kurtosis-based metrics outperformed diffusion-based metrics in this study. We found no significant differences in diffusion or kurtosis metrics between symptomatic and non-symptomatic hemispheres. In the context of the significant group differences, this indicates that abnormal diffusion kurtosis is present in the motor cortex in early ALS bilaterally.

The iron concentration and blood flow measurements were also compared between groups. We hypothesised that there would be a measurable increase in motor cortex iron concentration in ALS, thought to result from cell death (Andersen et al., 2014). In agreement with two previous studies, we found significantly greater iron concentrations in ALS compared to controls (Schweitzer et al., 2015; Costagli et al., 2016). We hypothesised a reduced blood flow in the motor cortex reflecting reduced metabolic demand or dysregulation of flow but did not observe any significant difference. This may indicate either that flow is not altered in early ALS, that it is altered by too small of a magnitude to confer a significant difference in our sample or that we could not observe a significant difference for methodological reasons; e.g., partial volume effects or the relatively short post-label delay. Previous studies of glucose metabolism and CBF in ALS using PET have been equivocal, reporting reductions in flow not specific to the motor cortex (Dalakas et al., 1987) or mild hypometabolism in small samples (Hatazawa et al., 1988), which are less-evident with shorter disease durations (Endo et al., 2017).

Imaging measures were only mildly related to disease severity, which may be partly ascribed to the relatively small spread and non-normal distributions of clinical variables in our sample. There was a trend toward an association between ALSFRS-R scores and a linear combination of the AKC and RK metrics, which were both decreased in more severely-impaired patients. While further interpretation of this relationship is not substantiated, we note that previous studies have shown relationships between disease status and kurtosis metrics in GM (Hori et al., 2014; Cauter et al., 2012; Bester et al., 2015). For disease duration, a strong linear relationship was found with motor cortex volume, at a rate of 1 mL GM loss per year in early ALS. A second strong relationship was found between disease duration and ADC, which has not been previously measured in the motor cortex GM in ALS, to our knowledge. This is consistent with a higher magnitude of overall diffusion without respect to directionality, indicating a general lack of cellularity and reduced integrity of membranes. We were not able to replicate the finding of decreased blood flow in a previous study (Rule et al., 2010), although the authors did not fully assess the motor cortex involvement. Nor did we find any significant relationships between FVC and any of the imaging measures. However, it should be considered that microstructural changes in the brain tissue represent multiple interacting processes that may be non-linear with respect to disease progression. Thus, a more detailed understanding is warranted of both the underlying cellular changes in neurodegeneration and how a future biophysical diffusion kurtosis model might reflect them, specifically in GM.

One limitation of our data was that the ASL acquisition used to measure CBF was suited to applications in brain regions with low arterial transit times. Since the sequence had a relatively short post-label delay and long label duration, it underestimated perfusion in regions with a long transit delay, such as in the motor cortex (Cercignani et al., 2018). While this underestimation was systematic and consistent across our sample, it does mean that our CBF values appear low in comparison to other similar studies. On the other hand, our ASL images were of a much greater spatial resolution than previous studies (Rule et al., 2010), allowing for more precise delineation of structures and a reduced partial volume effect. A short post-label delay was required to achieve a good SNR at such a high resolution. Future studies will apply a more refined experimental approach in order to improve these measurements.

Improved correction of partial volume effects may be obtained using

pulse sequences specifically designed for that purpose, rather than post-hoc correction. For example, a FLAIR-prepared diffusion acquisition or choice of a non-zero minimum b-value to suppress CSF (Salminen et al., 2016). While these approaches may improve accuracy of diffusion and kurtosis scalar measurements, our data acquisition was optimised toward reduced scan times and patient comfort over advanced partial volume correction techniques.

The generalisability of our findings depends on the extent to which our sample represents the early ALS population. Within the ALS group, ALSFRS-R scores indicated mild-to-moderate impairment, with a mean score of 40.2. The difference of this mean from the maximum possible score is comparable to reported minimal clinically-important differences of 6.7 (Miano et al., 2004) and 4.0 (Castrillo-Viguera et al., 2010). The ALS group's mean predicted FVC of 83% was in accordance with a previous study reporting predicted FVC at initial clinical presentation (80%; (Fallat et al., 1987)) but was also within the expected normal range for our sample's age group of ~70–130% (Stanojevic et al., 2008). Symptom onset was mostly in the right limb (which may be expected for the upper-limb onset patients, given that the cohort were all right-handed (Turner et al., 2011)) and the cohort was mostly male (expected given reported ALS prevalence (McCombe and Henderson, 2010)). We conclude from this that the sample is representative of early-to-middle stage ALS patients in general.

Finally, while we only report on GM changes here, it will also be important to test DKI changes in white matter. While the degenerative process is thought to begin in the cell bodies (Blizzard et al., 2015), the subsequent effects may be more accurately measured in white matter due to its more isotropic and less-noisy diffusion profile. Further interrogation of DKI changes in the CSTs is ongoing.

We conclude that state-of-the-art MRI measurements may be useful in providing complimentary information about tissue microstructure in early ALS. Translation of these techniques requires testing in larger samples and development of interpretable metrics informed by biophysical models in order to conduct studies of diagnostic accuracy.

Acknowledgments

We thank Jeff Macintosh, Trong Dang and the other staff at the MRI facility at Macquarie Medical Imaging, Macquarie University Hospital, New South Wales, Australia. We also thank Georgia Smith, clinical trials coordinator, Macquarie University, and the patients with ALS and control subjects who participated in the study. Anja Brau, Scott Hinks, Tim O'Meara, Matt Middione, Ajit Shankaranarayanan from GE Healthcare are all thanked for their facilitation of this work. SMG acknowledges the support of the Parker-Hughes Bequest and the Heart Research Institute. DBR acknowledges the support of the generous donors to the MND Research Centre, Macquarie University (www.mq.edu.au/mnd).

References

Alexander, A.L., Lee, J.E., Lazar, M., Field, A.S., 2007. Diffusion tensor imaging of the brain. Neurotherapeutics 4 (3), 316–329.
Andersen, H.H., Johnsen, K.B., Moos, T., 2014. Iron deposits in the chronically inflamed central nervous system and contributes to neurodegeneration. Cell. Mol. Life Sci. 71 (9), 1607–1622.
Andersson, J.L., Sotiropoulos, S.N., 2016. An integrated approach to correction for off-resonance effects and subject movement in diffusion MR imaging. Neuroimage 125, 1063–1078.
Andersson, J.L., Skare, S., Ashburner, J., 2003. How to correct susceptibility distortions in spin-echo echo-planar images: application to diffusion tensor imaging. Neuroimage 20 (2), 870–888.
Bartels, C., Mertens, N., Hofer, S., et al., 2008. Callosal dysfunction in amyotrophic lateral sclerosis correlates with diffusion tensor imaging of the central motor system. Neuromuscul. Disord. 18 (5), 398–407.
Bede, P., Iyer, P.M., Finegan, E., Omer, T., Hardiman, O., 2017. Virtual brain biopsies in amyotrophic lateral sclerosis: diagnostic classification based on in vivo pathological patterns. NeuroImage 15, 653–658.
Bester, M., Jensen, J.H., Babb, J.S., et al., 2015. Non-Gaussian diffusion MRI of gray matter is associated with cognitive impairment in multiple sclerosis. Mult. Scler. 21 (7), 935–944.
Blizzard, C.A., Southam, K.A., Dawkins, E., et al., 2015. Identifying the primary site of pathogenesis in amyotrophic lateral sclerosis – vulnerability of lower motor neurons to proximal excitotoxicity. Dis. Models 8 (3), 215–224.
Brooks, B.R., 1994. El escorial world federation of neurology criteria for the diagnosis of amyotrophic lateral sclerosis. J. Neurol. Sci. 124, 96–107.
Castrillo-Viguera, C., Grasso, D.L., Simpson, E., Shefner, J., Cudkowicz, M.E., 2010. Clinical significance in the change of decline in ALSFRS-R. Amyotroph. Lateral Scler. 11 (1–2), 178–180.
Cauter, S.V., Veraart, J., Sijbers, J., et al., 2012. Gliomas: diffusion kurtosis MR imaging in grading. Radiology 263 (2), 492–501.
Cercignani, M., Dowell, N.G., Tofts, P.S., 2018. Quantitative MRI of the brain: principles of physical measurement, 2nd ed. CRC Press, Boca Raton, FL.
Chang, J., Lomen-Hoerth, C., Murphy, J., et al., 2005. A voxel-based morphometry study of patterns of brain atrophy in ALS and ALS/FTLD. Neurology 65 (1), 75–80.
Costagli, M., Donatelli, G., Biagi, L., et al., 2016. Magnetic susceptibility in the deep layers of the primary motor cortex in amyotrophic lateral sclerosis. NeuroImage 12, 965–969.
Dai, W., Robson, P.M., Shankaranarayanan, A., Alsop, D.C., 2012. Reduced resolution transit delay prescan for quantitative continuous arterial spin labeling perfusion imaging. Magn. Reson. Med. 67 (5), 1252–1265.
Dalakas, M.C., Hatazawa, J., Brooks, R.A., Di Chiro, G., 1987. Lowered cerebral glucose utilization in amyotrophic lateral sclerosis. Ann. Neurol. 22 (5), 580–586.
de Carvalho, M., Dengler, R., Eisen, A., et al., 2008. Electrodiagnostic criteria for diagnosis of ALS. Clin. Neurophysiol. 119 (3), 497–503.
Destrieux, C., Fischl, B., Dale, A., Halgren, E., 2010. Automatic parcellation of human cortical gyri and sulci using standard anatomical nomenclature. Neuroimage 53 (1), 1–15.
Endo, H., Sekiguchi, K., Ueda, T., Kowa, H., Kanda, F., Toda, T., 2017. Regional glucose hypometabolic spread within the primary motor cortex is associated with amyotrophic lateral sclerosis disease progression: a fluoro-deoxyglucose positron emission tomography study. eNeurologicalSci 6, 74–79.
Fallat, R.J., Norris, F.H., Holden, D., Kandal, K., Roggero, P.C., 1987. Respiratory monitoring and treatment: objective treatments using non-invasive measurements. Adv. Exp. Med. Biol. 209, 191–200.
Filippini, N., Douaud, G., Mackay, C., Knight, S., Talbot, K., Turner, M., 2010. Corpus callosum involvement is a consistent feature of amyotrophic lateral sclerosis. Neurology 75 (18), 1645–1652.
Foerster, B.R., Dwamena, B.A., Petrou, M., et al., 2013. Diagnostic accuracy of diffusion tensor imaging in amyotrophic lateral sclerosis: a systematic review and individual patient data meta-analysis. Acad. Radiol. 20 (9), 1099–1106.
Grieve, S.M., Menon, P., Korgaonkar, M.S., et al., 2015. Potential structural and functional biomarkers of upper motor neuron dysfunction in ALS. Amyotroph Lateral Scler. Frontotemporal Degener 17 (1–2), 85–92.
Hatazawa, J., Brooks, R.A., Dalakas, M.C., Mansi, L., Di Chiro, G., 1988. Cortical motor-sensory hypometabolism in amyotrophic lateral sclerosis: a PET study. J. Comput. Assist. Tomogr. 12 (4), 630–636.
Hecht, M., Fellner, F., Fellner, C., Hilz, M., Heuss, D., Neundörfer, B., 2001. MRI-FLAIR images of the head show corticospinal tract alterations in ALS patients more frequently than T2-, T1-and proton-density-weighted images. J. Neurol. Sci. 186 (1–2), 37–44.
Hori, M., Tsutsumi, S., Yasumoto, Y., et al., 2014. Cervical spondylosis: Evaluation of microstructural changes in spinal cord white matter and gray matter by diffusional kurtosis imaging. Magn. Reson. Imaging 32 (5), 428–432.
Jones, D.K., Horsfield, M.A., Simmons, A., 1999. Optimal strategies for measuring diffusion in anisotropic systems by magnetic resonance imaging. Magn. Reson. Med. 42 (3), 515–525.
Kiernan, M.C., Vucic, S., Cheah, B.C., et al., 2011. Amyotrophic lateral sclerosis. Lancet 377 (9769), 942–955.
Klein, S., Staring, M., Murphy, K., Viergever, M.A., Pluim, J.P., 2010. Elastix: a toolbox for intensity-based medical image registration. IEEE Trans. Med. Imaging 29 (1), 196–205.
Li, H.Q., Yin, B., Quan, C., et al., 2018. Evaluation of patients with relapsing-remitting multiple sclerosis using tract-based spatial statistics analysis: diffusion kurtosis imaging. BMC Neurol. 18 (1), 108.
Liu, J., Liu, T., de Rochefort, L., et al., 2012. Morphology enabled dipole inversion for quantitative susceptibility mapping using structural consistency between the magnitude image and the susceptibility map. Neuroimage 59 (3), 2560–2568.
McCombe, P.A., Henderson, R.D., 2010. Effects of gender in amyotrophic lateral sclerosis. Gend Med 7 (6), 557–570.
Miano, B., Stoddard, G., Davis, S., Bromberg, M., 2004. Inter-evaluator reliability of the ALS functional rating scale. Amyotroph. Lateral Scler. Motor Neuron Disord. 5 (4), 235–239.
Miller, R.G., Munsat, T.L., Swash, M., Brooks, B.R., 1999. Consensus guidelines for the design and implementation of clinical trials in ALS. J. Neurol. Sci. 169 (1–2), 2–12.
Qi, L., Han, D., Wu, E.X., 2009. Principal invariants and inherent parameters of diffusion kurtosis tensors. J. Math. Anal. Appl. 349 (1), 165–180.
Rajagopalan, V., Pioro, E.P., 2017. Differential involvement of corticospinal tract (CST) fibers in UMN-predominant ALS patients with or without CST hyperintensity: A diffusion tensor tractography study. NeuroImage 14, 574–579.
Roccatagliata, L., Bonzano, L., Mancardi, G., Canepa, C., Caponnetto, C., 2009. Detection of motor cortex thinning and corticospinal tract involvement by quantitative MRI in amyotrophic lateral sclerosis. Amyotroph. Lateral Scler. 10 (1), 47–52.
Rule, R.R., Schuff, N., Miller, R.G., Weiner, M.W., 2010. Gray matter perfusion correlates with disease severity in ALS. Neurology 74 (10), 821–827.
Sach, M., Winkler, G., Glauche, V., et al., 2004. Diffusion tensor MRI of early upper motor

neuron involvement in amyotrophic lateral sclerosis. Brain 127 (2), 340–350.
Sage, C.A., Peeters, R.R., Görner, A., Robberecht, W., Sunaert, S., 2007. Quantitative diffusion tensor imaging in amyotrophic lateral sclerosis. Neuroimage 34 (2), 486–499.
Salminen, L.E., Conturo, T.E., Bolzenius, J.D., Cabeen, R.P., Akbudak, E., Paul, R.H., 2016. Reducing csf partial volume effects to enhance diffusion tensor imaging metrics of brain microstructure. Technol Innov 18 (1), 5–20.
Schuster, C., Hardiman, O., Bede, P., 2016. Development of an automated mri-based diagnostic protocol for amyotrophic lateral sclerosis using disease-specific pathognomonic features: a quantitative disease-state classification study. PLoS ONE 11 (12) (e0167331-e0167331).
Schweitzer, A.D., Liu, T., Gupta, A., et al., 2015. Quantitative susceptibility mapping of the motor cortex in amyotrophic lateral sclerosis and primary lateral sclerosis. Am. J. Roentgenol. 204 (5), 1086–1092.
Shahim, P., Holleran, L., Kim, J.H., Brody, D.L., 2017. Test-retest reliability of high spatial resolution diffusion tensor and diffusion kurtosis imaging. Sci. Rep. 7 (1), 11141.
Sidak, Z., 1967. Rectangular confidence regions for the means of multivariate normal distributions. J. Am. Stat. Assoc. 62 (318), 626–633.
Sperl, J.I., Sprenger, T., Tan, E.T., Menzel, M.I., Hardy, C.J., Marinelli, L., 2017. Model-based denoising in diffusion-weighted imaging using generalized spherical deconvolution. Magn. Reson. Med. 78 (6), 2428–2438.
Sprenger, T., Sperl, J.I., Fernandez, B., et al., 2016. Bias and precision analysis of diffusional kurtosis imaging for different acquisition schemes. Magn. Reson. Med. 76 (6), 1684–1696.
Stanojevic, S., Wade, A., Stocks, J., et al., 2008. Reference ranges for spirometry across all ages: a new approach. Am. J. Respir. Crit. Care Med. 177 (3), 253–260.
Steven, A.J., Zhuo, J., Melhem, E.R., 2014. Diffusion kurtosis imaging: an emerging technique for evaluating the microstructural environment of the brain. Am. J. Roentgenol. 202 (1), W26–W33.
Struyfs, H., Van Hecke, W., Veraart, J., et al., 2015. Diffusion kurtosis imaging: a possible MRI Biomarker for AD diagnosis? J. Alzheimers Dis. 48 (4), 937–948.
Tan, E.T., Marinelli, L., Slavens, Z.W., King, K.F., Hardy, C.J., 2013. Improved correction for gradient nonlinearity effects in diffusion-weighted imaging. J. Magn. Reson. Imaging 38 (2), 448–453.
Tan, E.T., Marinelli, L., Sperl, J.I., Menzel, M.I., Hardy, C.J., 2015. Multi-directional anisotropy from diffusion orientation distribution functions. J. Magn. Reson. Imaging 41 (3), 841–850.
Tuch, D.S., 2004. Q-ball imaging. Magn. Reson. Med. 52 (6), 1358–1372.
Turner, M.R., Modo, M., 2010. Advances in the application of MRI to amyotrophic lateral sclerosis. Expert Opinion Med. Diagn. 4 (6), 483–496.
Turner, M.R., Hammers, A., Allsop, J., et al., 2007. Volumetric cortical loss in sporadic and familial amyotrophic lateral sclerosis. Amyotroph. Lateral Scler. 8 (6), 343–347.
Turner, M.R., Kiernan, M.C., Leigh, P.N., Talbot, K., 2009. Biomarkers in amyotrophic lateral sclerosis. Lancet Neurol. 8 (1), 94–109.
Turner, M.R., Wicks, P., Brownstein, C., et al., 2011. Concordance between site of onset and limb dominance in amyotrophic lateral sclerosis. J. Neurol. Neurosurg. Psychiatry 82 (8), 853–854.
Vågberg, M., Granåsen, G., Svenningsson, A., 2017. Brain parenchymal fraction in healthy adults—a systematic review of the literature. PLoS ONE 12 (1), e0170018.
Vucic, S., Rothstein, J.D., Kiernan, M.C., 2014. Advances in treating amyotrophic lateral sclerosis: insights from pathophysiological studies. Trends Neurosci. 37 (8), 433–442.
Zhuo, J., Xu, S., Hazelton, J., et al., 2012. Diffusion kurtosis as an in vivo imaging marker for reactive astrogliosis in traumatic brain injury. Neuroimage 59 (1), 467–477.